THE JOURNAL OF PHYSICAL CHEMISTRY Letters

Letter

Cite This: J. Phys. Chem. Lett. 2019, 10, 7817−7822

pubs.acs.org/JPCL

Cryogenic Ion Spectroscopy of the Green Fluorescent Protein Chromophore in Vacuo

Wyatt Zagorec-Marks,[†] Madison M. Foreman,[†] Jan R. R. Verlet,[‡] and J. Mathias Weber*[,†]

[†]JILA and Department of Chemistry, University of Colorado, Boulder, Colorado 80309-0440, United States

[‡]Department of Chemistry, Durham University, Durham, DH1 3LE, U.K.

Supporting Information

ABSTRACT: We present the spectrum of the $S_1 \leftarrow S_0$ transition of an anionic model for the chromophore of the green fluorescent protein *in vacuo* at cryogenic temperatures, showing previously unresolved vibrational features, and resolving the band origin at 20 930 cm^{-1} (477.8 nm) with unprecedented accuracy. The vibrational spectrum establishes that the molecule is in the *Z* isomer at low temperature. At increased temperature, the $S_1 \leftarrow S_0$ band shifts to the red, which we tentatively attribute to emergent population of the *E* isomer.

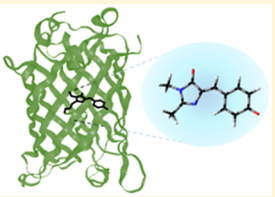

Fluorescent proteins have become a work-horse for fluorescence labeling in biology,[1−5] with the green fluorescent protein (GFP) and its variants being the most widely used for monitoring *in vivo* processes. The fluorescence originates from a small chromophore in the protein consisting of a phenol ring linked by a methine bridge at the *para*-position to an imidazole ring. The neutral and deprotonated (anionic) chromophores have absorption maxima around 395 and 480 nm, respectively,[6,7] but only the anion fluoresces as the neutral form undergoes excited state proton transfer.[7] A widely used model for the GFP chromophore is deprotonated *p*-hydroxybenzylidene-2,3-dimethylimidazolinone ($HBDI^-$, see Scheme 1), where the anchoring points to the protein are

Scheme 1. *Z* and *E* Isomers of $HBDI^-$

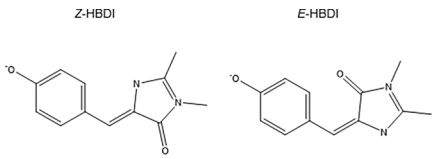

replaced by two methyl groups on the imidazole moiety. In contrast to the protein, $HBDI^-$[8−10] undergoes twisting around the bonds of the methine bridge during relaxation on the S_1 excited state in low-viscosity solvents[8,9] and *in vacuo*[10] and fluorescence is lost. The same twisting motions also give rise to two isomeric forms, *Z*-$HBDI^-$ and *E*-$HBDI^-$ (see Scheme 1). In fact, the Dronpa protein, which has the same chromophore as GFP, can be photoswitched between the fluorescent *Z* isomer and the nonfluorescent *E* isomer.[11,12]

The $S_1 \leftarrow S_0$ absorption profile contains details about the initial S_1 excited state photophysics of $HBDI^-$ and its interactions with the protein or solvent environment. Consequently, there have been many studies of $HBDI^-$ *in vacuo* in an attempt to understand the intrinsic photophysics. The first spectrum of isolated $HBDI^-$ showed striking similarities with the protein, suggesting that the sum of the interactions with the protein environment results in initial photophysics closer to vacuum than to aqueous solution. However, the photodissociation spectra presented to date have all been obtained at elevated temperature, obscuring many details of the intrinsic $S_1 \leftarrow S_0$ absorption profile.

The intrinsic photophysics of $HBDI^-$ has been mostly investigated through photodissociation and photoelectron spectroscopies,[8−10,13−36] as the relaxation from the S_1 excited state predominantly results in dissociation or electron loss. Photodissociation of bare $HBDI^-$ occurs after relaxation to the electronic ground state, which produces a vibrationally hot ion that decays primarily through the loss of a CH_3 group. For dissociation to be observable on a microsecond time scale, two photons in the visible spectral region need to be absorbed,[13] as one-photon dissociation occurs on a millisecond time scale.[15] Moreover, the threshold for electron detachment is only slightly higher (2.73 eV,[37] or 22 017 cm^{-1}) than the peak of the photodissociation spectrum at room temperature measured at around 480 nm (2.58 eV, or 20 833 cm^{-1}). As a result, electron detachment and dissociation are competing relaxation pathways upon photoexcitation, and detachment can proceed directly or through vibrational autodetachment, the latter of which is thought to dominate.[10,18−21,24,26−28,31] At 300 K, $HBDI^-$ stores ca. 390 meV in vibrational energy, which contributes to any statistical process. Hence, the interpretation of photodestruction experiments conducted to date has been complicated by a mixture of competing processes that have led to a debate in the literature since the first photodestruction spectrum of $HBDI^-$ was published in 2001.[13] Adding to this debate, a recent study by Bieske and co-workers[34] showed that under common preparation conditions, a significant fraction of the $HBDI^-$ ions is in the *E* isomeric form, while the interpretation of experimental data and computational efforts

Received: October 2, 2019
Accepted: November 4, 2019
Published: November 4, 2019

DOI: 10.1021/acs.jpclett.9b02916
J. Phys. Chem. Lett. 2019, 10, 7817−7822

have largely focused on the Z isomer. To overcome these ambiguities, here we present cryogenic spectra of bare and messenger-tagged $HBDI^-$ in the infrared and visible spectral regions, supported by density functional theory calculations. Our data show partially resolved vibrational structure of the $S_1 \leftarrow S_0$ transition of $HBDI^-$ and yields accurate values for the band origin. We demonstrate that $HBDI^-$ prepared at low temperature in a cryogenic ion trap exists predominantly as the Z isomer. With increasing temperature, the E isomer population increases.

Figure 1 shows the photodissociation action spectrum of the complex $[HBDI^-{\cdot}N_2]$, monitoring the formation of bare

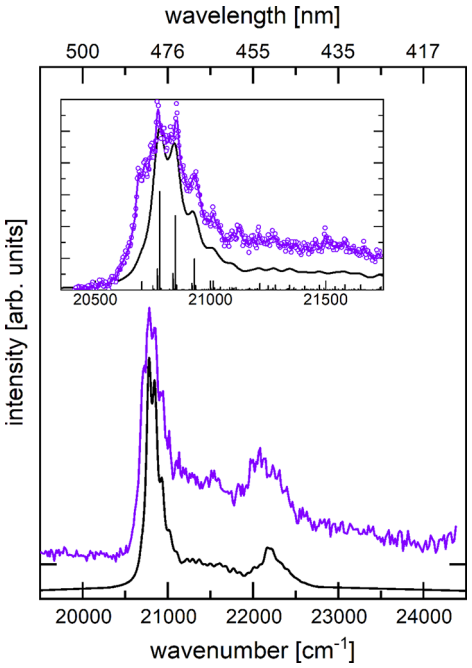

Figure 1. Photodissociation spectrum of $[HBDI^-{\cdot}N_2]$. The open circles are raw data points; the purple full line is a five-point adjacent average to guide the eye. The black full lines are Franck–Condon–Herzberg–Teller simulations of the vibrational substructure in the $S_1 \leftarrow S_0$ electronic band, with the vibrational states indicated as vertical sticks. The inset focuses on the band origin region, and the data in this trace were taken with a step size of 2.6 cm^{-1}, while the step size in the overview spectrum was 13 cm^{-1} in the origin region. The simulation has been shifted by ca. −4000 cm^{-1} for the best match to the experimental spectrum (see the Experimental and Computational Methods section).

$HBDI^-$ by the loss of the weakly bound N_2 messenger. Messenger loss can be expected to occur with near unit probability upon absorption of a photon down to the far-infrared, due to the low binding energy of N_2 (calculated at 630 cm^{-1} on the imidazole moiety, 720 cm^{-1} on the phenolate group). Consequently, the presence of N_2 guarantees that the target complexes are cold. The ion temperature can be conservatively estimated to be <75 K by describing cluster formation in the trap as an evaporative ensemble.[38] The spectrum of $[HBDI^-{\cdot}N_2]$ shows a sharp onset of the photodissociation action signal at (20530 ± 25) cm^{-1}, followed by a peak at (20780 ± 10) cm^{-1}, and a second peak at (20835 ± 10 cm^{-1}). Partially resolved vibrational structure is observed in the spectrum with a spacing of ca. 70 cm^{-1}. An additional feature appears with an onset at 21 830 cm^{-1} and a peak at 22 130 cm^{-1}.

To address which isomer is probed, the infrared spectrum of $[HBDI^-{\cdot}N_2]$ is shown in Figure 2, together with computed

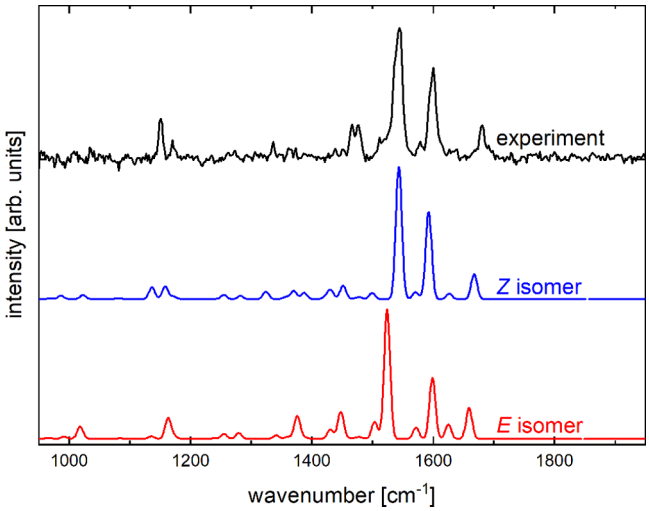

Figure 2. Experimental infrared action spectrum of $[HBDI^-{\cdot}N_2]$ (top trace) compared to simulated spectra of the Z isomer (center trace) and E isomer (bottom trace) of $HBDI^-$. The scaling factor for the simulated spectra is 0.98. A detailed assignment of the vibrational features is listed in Table S1 (see Supporting Information).

spectra of the Z and E isomers (scaled harmonic approximation). Although the predicted spectra of the two isomers are very similar, the spacings between the three most intense features in the 1400–1700 cm^{-1} region are distinctly different and match most closely with the Z isomer.[39] The narrow width of the main features indicates that only one isomer is significantly populated. The assignment is also consistent with calculations that place the Z isomer lower in energy by 100 meV, and with ion mobility experiments that showed only Z isomers for complexed $HBDI^-$ with solvent molecules.[34]

Figure 1 includes a Franck–Condon–Herzberg–Teller simulation of the $S_1 \leftarrow S_0$ band of the Z isomer (shifted to fit the experimental spectrum). The simulation qualitatively recovers the vibrational substructure of the experimental spectrum. The observed quantitative differences are not surprising given the level of theory, and they highlight the opportunity for high-level calculations to recover the S_1 potential energy surface in the Franck–Condon region. The qualitative agreement nevertheless enables us to assign general features. The low-frequency mode (ca. 70 cm^{-1}) corresponds to a methine bridge bending/ring scissoring mode (ω_B, calculated at ca. 80 cm^{-1} on the S_1 surface). We assign the peak at (20 780 ± 10) cm^{-1} as the electronic band origin, i.e., as the $S_1(v = 0) \leftarrow S_0(v = 0)$ transition of $[HBDI^-{\cdot}N_2]$, based on the hot band structure on its low-energy side. The broad feature beginning at ca. 21 830 cm^{-1} and peaking at (22 130 ± 40) cm^{-1} can be traced to combination bands of ω_B building on an imidazole ring breathing/in-plane CH bending mode on the S_1 surface (ω_I, calculated at ca. 1350 cm^{-1}), in accord with previous assignments.[22,40,41] Congestion in the spectrum is largely caused by the Franck–Condon active ω_B mode, which is also responsible for the two hot band shoulders below the band origin and the high-energy shoulder on the feature belonging to ω_I. Both ω_B and ω_I have been identified as

DOI: 10.1021/acs.jpclett.9b02916
J. Phys. Chem. Lett. 2019, 10, 7817–7822

strongly Franck−Condon active modes in earlier computational work, and our calculated spectral profile qualitatively agrees with results from other calculations at much higher levels of theory (see the Supporting Information).[22,40,41]

Note that the width of the experimental vibrational signatures is not limited by the experiment (see the Experimental and Computational Methods section), which is on the order of ca. 5−10 cm^{-1}.[42] Our simulation suggests that the measured line width has a full width at half-maximum of about 80 cm^{-1}. This broadening is in part due to congestion from other low-frequency modes and due to the intrinsic dynamics on the S_1 state leading to lifetime broadening.

The spectrum in Figure 1 is that of $[HBDI^-{\cdot}N_2]$, but the species of interest is bare $HBDI^-$. Previous experiments using N_2 as a messenger tag[43] suggest that the presence of the N_2 tag leads to a small overall spectral shift at the same ion trap temperature. The photodissociation spectrum of bare $HBDI^-$ at various trap temperatures is shown in Figure 3 and is compared to the spectrum of $[HBDI^-{\cdot}N_2]$. These spectra were acquired by monitoring the loss of CH_3, which is assumed to be a two-photon process, as the observation time in our experiment is ca. 20 μs.

The spectrum of bare $HBDI^-$ at 30 K has an onset at (20 250 ± 50) cm^{-1}, which is at much lower wavenumbers than that of $[HBDI^-{\cdot}N_2]$, and the peak of the spectrum is at (20 930 ± 10) cm^{-1}, with partially resolved peaks at lower energies. At the high-energy side of this peak, vibrational features are observed, with a spacing commensurate with that found in the spectrum of $[HBDI^-{\cdot}N_2]$. We assign the peak at 20 930 cm^{-1} (ca. 477.8 nm) to the $S_1(v = 0) \leftarrow S_0(v = 0)$ transition of bare $HBDI^-$.

The presence of the first N_2 tag shifts the spectrum by (150 ± 27) cm^{-1} to the red; a second N_2 tag leads to an additional (80 ± 27) cm^{-1} red shift (measured from the highest point in the band envelope; see the Supporting Information). Interestingly, the peak in the spectrum of wild-type GFP at 77 K is found at (21 230 ± 100) cm^{-1},[7] resulting in a shift of the peak by the protein environment by +300 cm^{-1} (see Figure 4). With increasing temperature, a prominent shoulder below the band origin develops at 180 K into a partially resolved peak at (20 700 ± 25) cm^{-1} (483.1 nm), which dominates the spectrum at 300 K. This low-energy features could be due to hot bands. However, our Franck−Condon simulations do not recover the observed evolution of a second discernible low-energy peak, regardless of the simulation temperature, consistent with Franck−Condon simulations by others.[22,40,41] Alternatively, this low-energy peak could be due to the presence of the *E* isomer. Recent results by Bieske and co-workers observed the presence of the *E* isomer in ion mobility experiments on $HBDI^-$ ions prepared at room temperature[34] and presented evidence that the *E* isomer absorbs at slightly longer wavelengths than the *Z* isomer. The barrier to interconversion has been calculated to be 1.24 eV, which would hinder thermal isomerization.[34] Nonetheless, while there remains some ambiguity regarding the origin of the low-energy feature, we tentatively ascribe it to the presence of the *E* isomer. Similar to the electronic band origin, the feature around 22 000 cm^{-1} broadens and red-shifts with increasing temperature. We attribute this effect to the *E* isomer having overall a similar Franck−Condon progression as the *Z* isomer (see the Supporting Information).

Subtle differences between the envelope of the spectra of bare and N_2-tagged $HBDI^-$ warrant some consideration. The relative intensities of the feature around 22 000 cm^{-1} and of the $S_1(v = 0) \leftarrow S_0(v = 0)$ band are different for $[HBDI^-{\cdot}N_2]$ compared to bare $HBDI^-$. This difference could be due to a change in the Franck−Condon factors upon addition of an N_2 tag, although this seems unlikely given the small perturbation that the N_2 tag induces. Alternatively, it could be caused by a change in the branching ratio of internal conversion versus electron detachment. The adiabatic electron affinity of HBDI is 22 017 cm^{-1}.[37] Moreover, vibrational autodetachment from the S_1 state has been observed to be a significant decay channel in $HBDI^-$ (at 300 K) excited at 19 600 cm^{-1} and higher.[10,18−21,24,26−28,31] However, a direct comparison of parent ion depletion and fragment action for bare $HBDI^-$ shows that

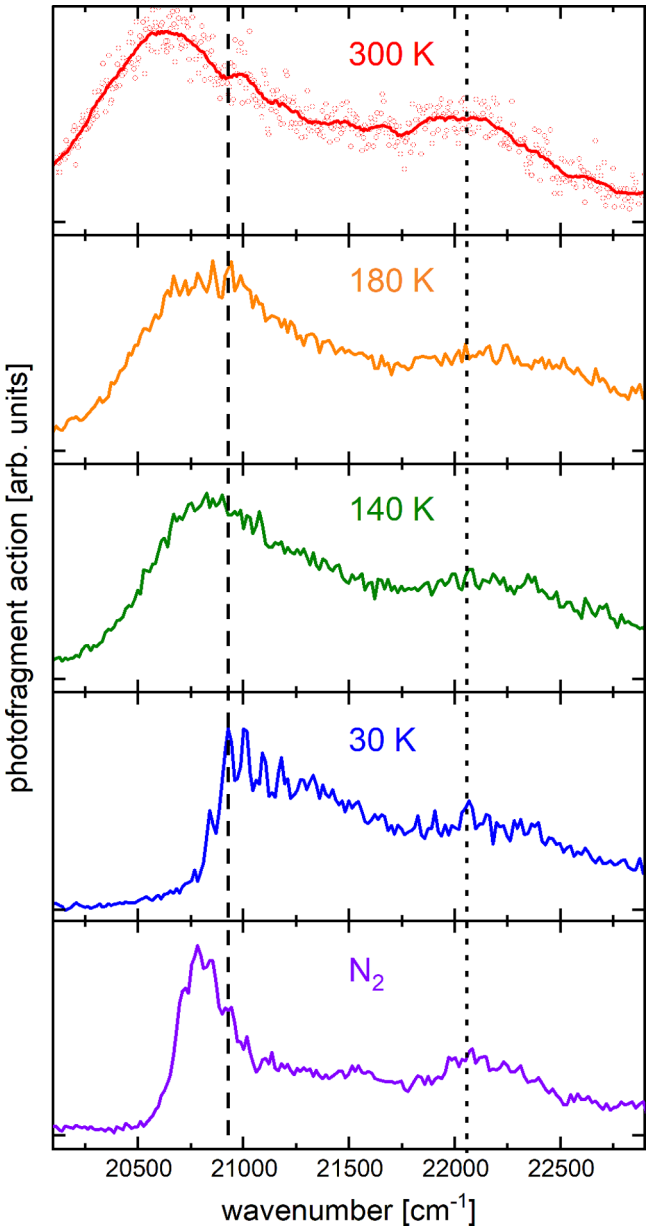

Figure 3. Photodissociation spectra of $HBDI^-$ at different trap temperatures. For the spectrum at 300 K, the open circles are raw data points and the full line is a 20-point adjacent average to guide the eye. For the other spectra, the solid line represents the raw data. The vertical dashed and dotted lines show the peak positions for bare $HBDI^-$ (30 K) of the $(v = 0) \leftarrow (v = 0)$ band at (20 930 ± 10) cm^{-1}, and of the high-energy feature around 22 100 cm^{-1}, respectively.

DOI: 10.1021/acs.jpclett.9b02916
J. Phys. Chem. Lett. 2019, 10, 7817−7822

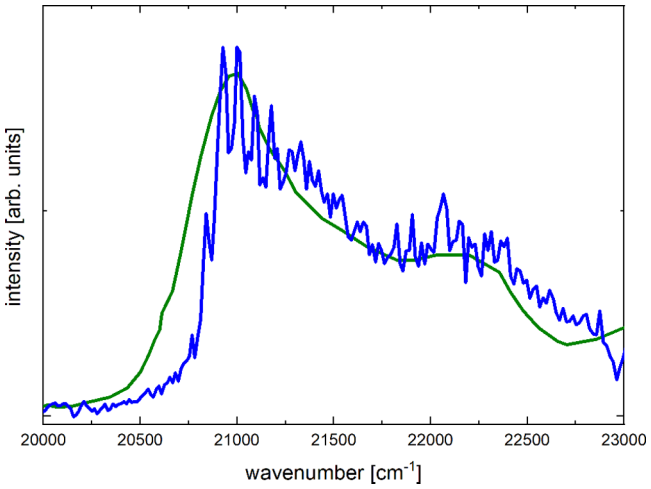

Figure 4. Comparison of the experimental spectrum of $HBDI^-$ at 30 K trap temperature (blue line) with the absorption spectrum of wild-type GFP (green line). The absorption spectrum of wild-type GFP shown here represents the deconvoluted absorption spectrum attributed to the deprotonated state of the chromophore (digitized from Figure 2a in ref 7). The wild-type GFP spectrum has been shifted by -300 cm^{-1} to optimally match the experimental spectrum of $HBDI^-$.

electron detachment does not significantly contribute to the photodestruction of the ion at 30 K trap temperature (see the Supporting Information). The overall band contour of the spectrum of cryogenically prepared $HBDI^-$ also compares very well with the absorption spectrum of wild-type GFP at 77 K (see Figure 4),[7,44] for which photodetachment is not possible in the visible, suggesting that photodetachment plays only a minor role at low temperatures in the spectral range probed here. We suggest that the change in the envelope of the spectrum could be caused by differences in *ion* temperature between $[HBDI^-{\cdot}N_2]$ and bare $HBDI^-$ despite similar *trap* temperatures. The presence of the N_2 tag limits the internal energy of the complex to a maximum of ca. 720 cm^{-1}, which is not the case for the bare ion, and radio-frequency heating could introduce hot bands in the bare ion that are quenched by the presence of an N_2 tag.

Summarizing, we have removed many of the ambiguities in the photodissociation action spectrum of the chromophore of GFP by performing experiments on ions prepared in a cryogenic ion trap. The $S_1(v = 0) \leftarrow S_0(v = 0)$ transition of *Z*-$HBDI^-$ is at $(20\,930 \pm 15)$ cm^{-1}, and the band shows partially resolved vibrational structures that are assigned to specific Franck–Condon active modes. At higher ion temperatures, it is likely that the *E* isomer of $HBDI^-$ is observed, tentatively assigning its $S_1(v = 0) \leftarrow S_0(v = 0)$ transition to a feature that is red-shifted by (230 ± 30) cm^{-1} compared to the *Z* isomer. At room temperature, this low-energy feature is dominant in our experiment. These results highlight the importance of acquiring action spectra under well-controlled conditions and suggests that previous studies on $HBDI^-$ may need to be revisited. Finally, the high-resolution spectrum measured here serves as a benchmark for theoretical studies that can now provide detailed insight into the S_1 state of *Z*-$HBDI^-$ in the Franck–Condon region.

Experimental and Computational Methods. Solutions were prepared by dissolving HBDI in methanol with the pH adjusted to 11–12 by adding a few drops of aqueous KOH (ca. 50 mM), resulting in a dark yellow to orange solution. The solution was electrosprayed without further purification using N_2 as the nebulizing gas. The spray enters a heated desolvation capillary at the entrance of a sequence of differential pumping stages where residual solvent molecules are evaporated, resulting in bare ions. After leaving the heated capillary, the ions pass through a set of skimmers and a series of octopole ion guides before injection into a 3D quadrupole ion trap. This ion trap is mounted on a closed cycle helium cryostat and is equipped with a resistive heater to allow temperature control from room temperature down to 20 K. The ions are stored in this trap with D_2 buffer gas for 100 ms to cool them to cryogenic temperatures. In the cryogenic ion trap, we form complexes of $[HBDI^-{\cdot}(N_2)_n]$ ($n = 0$–2). The complexes are injected into a time-of-flight mass spectrometer where we mass select target ions using a pulsed mass gate. These mass selected ions are then irradiated with the output of a tunable optical parametric converter with pulse durations of 5–7 ns. The light source for spectroscopy in the visible spectral range is a BBO based optical parametric oscillator with a bandwidth of ca. 5 cm^{-1}. For infrared spectroscopy we use a KTP/KTA/$AgGaSe_2$ based optical parametric converter system with a bandwidth of ca. 2 cm^{-1}. Fragmentation upon absorption of a photon is monitored using a reflectron for secondary mass analysis with a microchannel plate detector for fragment ion detection. Care was taken to ensure that the laser pulse energies used were sufficiently low to avoid significant multiphoton absorption.

The mass spectrometer was operated at a repetition rate of 10 Hz, and the light source was fired every other cycle to allow subtraction of background from unimolecular decay by monitoring of fragment ion signal with and without the laser. All spectra were corrected for photon fluence, where the spectra of $[HBDI^-{\cdot}N_2]$ were corrected assuming a one-photon process, while spectra of bare $HBDI^-$ were corrected assuming that the dissociation is a two-photon process.

Geometry optimizations and harmonic frequency calculations for the ground state were carried out using density functional theory (DFT) with the B3LYP functional[45] with a def2-TZVPP basis set[46] for all atoms. As previously noted by others, there is a strong basis set dependence of the IR features,[39] but we found in exploratory calculations that this problem only occurs for smaller basis sets than the one used here. Excited states were calculated using the range-corrected CAM-B3LYP functional.[47] Franck–Condon simulations were performed by using results from the excited state calculations. The simulation temperature is 55 K, the full width at half-maximum (fwhm) of the vibrational features is 80 cm^{-1}, and the frequency ω_B was set to 65 cm^{-1} on the S_1 surface to fit the observed vibrational structure. Vertical excitation calculations using both CAM-B3LYP and ω-B97X-D[48] functionals yield similar results that overestimate the electronic band origin by about 0.5 eV for the *Z* isomer. We shifted the calculated vertical excitation energies by ca. -4000 cm^{-1} to match the calculated vibronic progression with the experimental spectrum of $[HBDI^-{\cdot}N_2]$. All calculations were carried out in Gaussian 16.[49]

■ ASSOCIATED CONTENT

Supporting Information

The Supporting Information is available free of charge at https://pubs.acs.org/doi/10.1021/acs.jpclett.9b02916.

DOI: 10.1021/acs.jpclett.9b02916
J. Phys. Chem. Lett. 2019, 10, 7817–7822

Vibrational mode assignments for $[HBDI^{-}\cdot N_2]$; comparison of the experimental spectrum of $[HBDI^{-}\cdot N_2]$ with calculated spectra from the literature; photodissociation action spectrum of $[HBDI^{-}\cdot(N_2)_2]$; Franck−Condon simulation of the $S_1 \leftarrow S_0$ transition of the *E* isomer of $HBDI^{-}$; comparison of action and depletion spectra for $HBDI^{-}$; optimized geometry of the ground state of the *Z* isomer; optimized geometry of the S_1 state of the *Z* isomer; optimized geometry of the ground state of the *E* isomer; optimized geometry of the S_1 state of the *E* isomer; calculated vibrational frequencies (unscaled) in cm^{-1} (PDF)

AUTHOR INFORMATION

Corresponding Author

*E-mail: weberjm@jila.colorado.edu. Tel: +1-303-492-7841.

ORCID

Jan R. R. Verlet: 0000-0002-9480-432X

J. Mathias Weber: 0000-0002-5493-5886

Notes

The authors declare no competing financial interest.

ACKNOWLEDGMENTS

We gratefully acknowledge support from the U.S. National Science Foundation under award no. CHE-1764191, the NSF Physics Frontier Center at JILA (award no. PHY-1734006), and JILA for a Visiting Fellowship to J.R.R.V. We also thank Drs. Stephen R. Meech and Philip C. B. Page (University of East Anglia, UK, grant support through EPSCR grants EP/E010466 and EP/H025715) for providing us with the *p*-hydroxybenzylidene-2,3-dimethylimidazolinone samples that were used in this work.

REFERENCES

(1) Chalfie, M.; Tu, Y.; Euskirchen, G.; Ward, W. W.; Prasher, D. C. Green fluorescent protein as a marker for gene-expression. *Science* **1994**, *263*, 802−805.

(2) Tsien, R. Y. The green fluorescent protein. *Annu. Rev. Biochem.* **1998**, *67*, 509−544.

(3) Hein, B.; Willig, K. I.; Hell, S. W. Stimulated emission depletion (STED) nanoscopy of a fluorescent protein-labeled organelle inside a living cell. *Proc. Natl. Acad. Sci. U. S. A.* **2008**, *105*, 14271−14276.

(4) Day, R. N.; Davidson, M. W. The fluorescent protein palette: tools for cellular imaging. *Chem. Soc. Rev.* **2009**, *38*, 2887−2921.

(5) Chudakov, D. M.; Matz, M. V.; Lukyanov, S.; Lukyanov, K. A. Fluorescent proteins and their applications in imaging living cells and tissues. *Physiol. Rev.* **2010**, *90*, 1103−1163.

(6) Heim, R.; Prasher, D. C.; Tsien, R. Y. Wavelength mutations and posttranslational autooxidation of green fluorescent protein. *Proc. Natl. Acad. Sci. U. S. A.* **1994**, *91*, 12501−12504.

(7) Chattoraj, M.; King, B. A.; Bublitz, G. U.; Boxer, S. G. Ultra-fast excited state dynamics in green fluorescent protein: Multiple states and proton transfer. *Proc. Natl. Acad. Sci. U. S. A.* **1996**, *93*, 8362−8367.

(8) Mandal, D.; Tahara, T.; Meech, S. R. Excited-state dynamics in the green fluorescent protein chromophore. *J. Phys. Chem. B* **2004**, *108*, 1102−1108.

(9) Litvinenko, K. L.; Webber, N. M.; Meech, S. R. Internal conversion in the chromophore of the green fluorescent protein: Temperature dependence and isoviscosity analysis. *J. Phys. Chem. A* **2003**, *107*, 2616−2623.

(10) Forbes, M. W.; Jockusch, R. A. Deactivation pathways of an isolated green fluorescent protein model chromophore studied by electronic action spectroscopy. *J. Am. Chem. Soc.* **2009**, *131*, 17038−17039.

(11) Voliani, V.; Bizzarri, R.; Nifosi, R.; Abbruzzetti, S.; Grandi, E.; Viappiani, C.; Beltram, F. Cis-trans photoisomerization of fluorescent-protein chromophores. *J. Phys. Chem. B* **2008**, *112*, 10714−10722.

(12) Kaucikas, M.; Tros, M.; van Thor, J. J. Photoisomerization and proton transfer in the forward and reverse photoswitching of the fast-switching M159T mutant of the Dronpa fluorescent protein. *J. Phys. Chem. B* **2015**, *119*, 2350−2362.

(13) Nielsen, S. B.; Lapierre, A.; Andersen, J. U.; Pedersen, U. V.; Tomita, S.; Andersen, L. H. Absorption spectrum of the green fluorescent protein chromophore anion in vacuo. *Phys. Rev. Lett.* **2001**, *87*, 228102.

(14) Andersen, L. H.; Lapierre, A.; Nielsen, S. B.; Nielsen, I. B.; Pedersen, S. U.; Pedersen, U. V.; Tomita, S. Chromophores of the green fluorescent protein studied in the gas phase. *Eur. Phys. J. D* **2002**, *20*, 597−600.

(15) Andersen, L. H.; Bluhme, H.; Boye, S.; Jorgensen, T. J. D.; Krogh, H.; Nielsen, I. B.; Nielsen, S. B.; Svendsen, A. Experimental studies of the photophysics of gas-phase fluorescent protein chromophores. *Phys. Chem. Chem. Phys.* **2004**, *6*, 2617−2627.

(16) Lammich, L.; Petersen, M. A.; Nielsen, M. B.; Andersen, L. H. The gas-phase absorption spectrum of a neutral GFP model chromophore. *Biophys. J.* **2007**, *92*, 201−207.

(17) Chingin, K.; Balabin, R. M.; Frankevich, V.; Barylyuk, K.; Nieckarz, R.; Sagulenko, P.; Zenobi, R. Absorption of the green fluorescent protein chromophore anion in the gas phase studied by a combination of FTICR mass spectrometry with laser-induced photodissociation spectroscopy. *Int. J. Mass Spectrom.* **2011**, *306*, 241−245.

(18) Forbes, M. W.; Nagy, A. M.; Jockusch, R. A. Photofragmentation of and electron photodetachment from a GFP model chromophore in a quadrupole ion trap. *Int. J. Mass Spectrom.* **2011**, *308*, 155−166.

(19) Horke, D. A.; Verlet, J. R. R. Photoelectron spectroscopy of the model GFP chromophore anion. *Phys. Chem. Chem. Phys.* **2012**, *14*, 8511−8515.

(20) Mooney, C. R. S.; Sanz, M. E.; McKay, A. R.; Fitzmaurice, R. J.; Aliev, A. E.; Caddick, S.; Fielding, H. H. Photodetachment spectra of deprotonated fluorescent protein chromophore anions. *J. Phys. Chem. A* **2012**, *116*, 7943−7949.

(21) Toker, Y.; Rahbek, D. B.; Klaerke, B.; Bochenkova, A. V.; Andersen, L. H. Direct and indirect electron emission from the green fluorescent protein chromophore. *Phys. Rev. Lett.* **2012**, *109*, 128101.

(22) Bochenkova, A. V.; Andersen, L. H. Ultrafast dual photoresponse of isolated biological chromophores: link to the photoinduced mode-specific non-adiabatic dynamics in proteins. *Faraday Discuss.* **2013**, *163*, 297−319.

(23) Mooney, C. R. S.; Horke, D. A.; Chatterley, A. S.; Simperler, A.; Fielding, H. H.; Verlet, J. R. R. Taking the green fluorescence out of the protein: dynamics of the isolated GFP chromophore anion. *Chem. Sci.* **2013**, *4*, 921−927.

(24) West, C. W.; Hudson, A. S.; Cobb, S. L.; Verlet, J. R. R. Communication: Autodetachment versus internal conversion from the S_1 state of the isolated GFP chromophore anion. *J. Chem. Phys.* **2013**, *139*, No. 071104.

(25) Bochenkova, A. V.; Klaerke, B.; Rahbek, D. B.; Rajput, J.; Toker, Y.; Andersen, L. H. UV excited-state photoresponse of biochromophore negative ions. *Angew. Chem., Int. Ed.* **2014**, *53*, 9797−9801.

(26) Mooney, C. R. S.; Parkes, M. A.; Zhang, L. J.; Hailes, H. C.; Simperler, A.; Bearpark, M. J.; Fielding, H. H. Competition between photodetachment and autodetachment of the 2 $^1\pi\pi^*$ state of the green fluorescent protein chromophore anion. *J. Chem. Phys.* **2014**, *140*, 205103.

(27) West, C. W.; Bull, J. N.; Hudson, A. S.; Cobb, S. L.; Verlet, J. R. R. Excited State Dynamics of the isolated green fluorescent protein chromophore anion following UV excitation. *J. Phys. Chem. B* **2015**, *119*, 3982−3987.

DOI: 10.1021/acs.jpclett.9b02916
J. Phys. Chem. Lett. 2019, 10, 7817−7822

(28) Anstöter, C. S.; Bull, J. N.; Verlet, J. R. R. Ultrafast dynamics of temporary anions probed through the prism of photodetachment. *Int. Rev. Phys. Chem.* **2016**, *35*, 509−538.
(29) Kiefer, H. V.; Pedersen, H. B.; Bochenkova, A. V.; Andersen, L. H. Decoupling electronic versus nuclear photoresponse of isolated green fluorescent protein chromophores using short laser pulses. *Phys. Rev. Lett.* **2016**, *117*, 243004.
(30) Anstöter, C. S.; Dean, C. R.; Verlet, J. R. R. Chromophores of chromophores: a bottom-up Hückel picture of the excited states of photoactive proteins. *Phys. Chem. Chem. Phys.* **2017**, *19*, 29772−29779.
(31) Bochenkova, A. V.; Mooney, C. R. S.; Parkes, M. A.; Woodhouse, J. L.; Zhang, L. J.; Lewin, R.; Ward, J. M.; Hailes, H. C.; Andersen, L. H.; Fielding, H. H. Mechanism of resonant electron emission from the deprotonated GFP chromophore and its biomimetics. *Chem. Sci.* **2017**, *8*, 3154−3163.
(32) McLaughlin, C.; Assmann, M.; Parkes, M. A.; Woodhouse, J. L.; Lewin, R.; Hailes, H. C.; Worth, G. A.; Fielding, H. H. ortho and para chromophores of green fluorescent protein: controlling electron emission and internal conversion. *Chem. Sci.* **2017**, *8*, 1621−1630.
(33) Tay, J.; Parkes, M. A.; Addison, K.; Chan, Y. H.; Zhang, L. J.; Hailes, H. C.; Page, P. C. B.; Meech, S. R.; Blancafort, L.; Fielding, H. H. The Effect of conjugation on the competition between internal conversion and electron detachment: a comparison between green fluorescent and red Kaede protein chromophores. *J. Phys. Chem. Lett.* **2017**, *8*, 765−771.
(34) Carrascosa, E.; Bull, J. N.; Scholz, M. S.; Coughlan, N. J. A.; Olsen, S.; Wille, U.; Bieske, E. J. Reversible photoisomerization of the isolated green fluorescent protein chromophore. *J. Phys. Chem. Lett.* **2018**, *9*, 2647−2651.
(35) Langeland, J.; Kjaer, C.; Andersen, L. H.; Nielsen, S. B. The effect of an electric field on the spectroscopic properties of the isolated green fluorescent protein chromophore anion. *ChemPhysChem* **2018**, *19*, 1686−1690.
(36) Henley, A.; Fielding, H. H. Anion photoelectron spectroscopy of protein chromophores. *Int. Rev. Phys. Chem.* **2019**, *38*, 1−34.
(37) Deng, S. H. M.; Kong, X. Y.; Zhang, G. X.; Yang, Y.; Zheng, W. J.; Sun, Z. R.; Zhang, D. Q.; Wang, X. B. Vibrationally resolved photoelectron spectroscopy of the model GFP chromophore anion revealing the photoexcited S_1 state being both vertically and adiabatically bound against the photodetached D_0 continuum. *J. Phys. Chem. Lett.* **2014**, *5*, 2155−2159.
(38) Klots, C. E. Temperatures of evaporating clusters. *Nature* **1987**, *327*, 222−223.
(39) Almasian, M.; Grzetic, J.; Berden, G.; Bakker, B.; Buma, W. J.; Oomens, J. Gas-phase infrared spectrum of the anionic GFP-chromophore. *Int. J. Mass Spectrom.* **2012**, *330*, 118−123.
(40) Martin, M. E.; Negri, F.; Olivucci, M. Origin, nature, and fate of the fluorescent state of the green fluorescent protein chromophore at the CASPT2//CASSCF resolution. *J. Am. Chem. Soc.* **2004**, *126*, 5452−5464.
(41) Kamarchik, E.; Krylov, A. I. Non-Condon effects in the one- and two-photon absorption spectra of the green fluorescent protein. *J. Phys. Chem. Lett.* **2011**, *2*, 488−492.
(42) Dodson, L. G.; Zagorec-Marks, W.; Xu, S.; Smith, J. E. T.; Weber, J. M. Intrinsic photophysics of nitrophenolate ions studied by cryogenic ion spectroscopy. *Phys. Chem. Chem. Phys.* **2018**, *20*, 28535−28543.
(43) Xu, S.; Smith, J. E. T.; Weber, J. M. The electronic spectrum of cryogenic ruthenium-tris-bipyridine dications in vacuo. *J. Chem. Phys.* **2016**, *145*, No. 024304.
(44) Bublitz, G.; King, B. A.; Boxer, S. G. Electronic structure of the chromophore in green fluorescent protein (GFP). *J. Am. Chem. Soc.* **1998**, *120*, 9370−9371.
(45) Becke, A. D. Density-Functional Exchange-energy approximation with correct asymptotic-behavior. *Phys. Rev. A: At., Mol., Opt. Phys.* **1988**, *38*, 3098−3100.
(46) Weigend, F.; Ahlrichs, R. Balanced basis sets of split valence, triple zeta valence and quadruple zeta valence quality for H to Rn: Design and assessment of accuracy. *Phys. Chem. Chem. Phys.* **2005**, *7*, 3297−3305.
(47) Yanai, T.; Tew, D. P.; Handy, N. C. A new hybrid exchange-correlation functional using the Coulomb-attenuating method (CAM-B3LYP). *Chem. Phys. Lett.* **2004**, *393*, 51−57.
(48) Chai, J.-D.; Head-Gordon, M. Long-range corrected hybrid density functionals with damped atom−atom dispersion corrections. *Phys. Chem. Chem. Phys.* **2008**, *10*, 6615−6620.
(49) Frisch, M. J.; Trucks, G. W.; Schlegel, H. B.; Scuseria, G. E.; Robb, M. A.; Cheeseman, J. R.; Scalmani, G.; Barone, V.; Petersson, G. A.; Nakatsuji, H.; Li, X.; Caricato, M.; Marenich, A. V.; Bloino, J.; Janesko, B. G.; Gomperts, R.; Mennucci, B.; Hratchian, H. P.; Ortiz, J. V.; Izmaylov, A. F.; Sonnenberg, J. L.; Williams; Ding, F.; Lipparini, F.; Egidi, F.; Goings, J.; Peng, B.; Petrone, A.; Henderson, T.; Ranasinghe, D.; Zakrzewski, V. G.; Gao, J.; Rega, N.; Zheng, G.; Liang, W.; Hada, M.; Ehara, M.; Toyota, K.; Fukuda, R.; Hasegawa, J.; Ishida, M.; Nakajima, T.; Honda, Y.; Kitao, O.; Nakai, H.; Vreven, T.; Throssell, K.; Montgomery, J. A., Jr.; Peralta, J. E.; Ogliaro, F.; Bearpark, M. J.; Heyd, J. J.; Brothers, E. N.; Kudin, K. N.; Staroverov, V. N.; Keith, T. A.; Kobayashi, R.; Normand, J.; Raghavachari, K.; Rendell, A. P.; Burant, J. C.; Iyengar, S. S.; Tomasi, J.; Cossi, M.; Millam, J. M.; Klene, M.; Adamo, C.; Cammi, R.; Ochterski, J. W.; Martin, R. L.; Morokuma, K.; Farkas, O.; Foresman, J. B.; Fox, D. J. *Gaussian 16* Rev. C.01; Gaussian, Inc.: Wallingford, CT, 2016.

DOI: 10.1021/acs.jpclett.9b02916
J. Phys. Chem. Lett. 2019, 10, 7817−7822